J. Fluid Mech. (1990), *vol.* 220, *pp.* 253–266
Printed in Great Britain

The effect of buoyancy on vortex shedding in the near wake of a circular cylinder

By KEUN-SHIK CHANG AND JONG-YOUB SA
Department of Aerospace Engineering, Korea Advanced Institute of Science and Technology, P.O. Box 150, Cheongryang, Seoul, Republic of Korea

(Received 28 July 1988 and in revised form 1 March 1990)

The phenomenon of vortex shedding from a heated/cooled circular cylinder has been investigated numerically in the mixed natural and forced convection regimes. Accuracy of the computation was achieved by the fourth-order Hermitian relation applied to the contravariant velocity components in the convection terms of the vorticity transport equation, and by the far-boundary stream-function condition of an integral-series form developed by the authors. Purely periodic flows at $Re = 100$, efficiently established through the use of a direct elliptic solver called the SEVP, was found to degenerate into a steady twin-vortex pattern at the critical Grashof number 1500, confirming an earlier experimental observation identified as 'breakdown of the Kármán vortex street'. Various other buoyancy effects about the heated/cooled cylinder are discussed by means of the flow patterns, the Nusselt number and the drag coefficient curves.

1. Introduction

The viscous flow past a circular cylinder has attracted much attention from fluid dynamicists, both experimentalists and theoreticians. A variety of vortex shedding characteristics have already been discussed in the literature in the Reynolds-number range 50–200; a good review is given by Berger & Wille (1972).

Vortex shedding in the mixed convection regime is physically more complicated owing to the buoyancy effect added to the viscous phenomena. The majority of papers in this area have treated steady-state mixed convection with the Reynolds number limited up to 40: for example, see Badr (1984). As one of a few exceptions, Oosthuizen & Madan (1971) studied experimentally mixed convection in the Reynolds number range 100–300 in which the flow was highly unsteady. Their interest was, however, in the average heat transfer, not in the detailed behaviour of the near-wake vortices, one of the objectives of the present paper. Noto & Matsumoto (1985, 1987*a*, *b*) have studied the development of the vortex cores in a Kármán vortex street behind a heated cylinder, including the degeneration of the unsteady vortices to the stationary ones; their investigation nevertheless lacks a detailed study on the vortex shedding mechanisms. Jain & Lohar (1979) and, additionally, Noto & Matsumoto (1987*a*) reported on the increase in vortex shedding frequency with increasing cylinder temperature. These studies were made only in a transient state well before a fully periodic state was assumed in the flow: $t \leqslant 20$ in Jain & Lohar (1979) and $t \leqslant 40$ in Noto & Matsumoto (1987*a*).

In the present paper, strictly periodic flows ($t \geqslant 200$) past a heated/cooled circular cylinder have been computed with a time-efficient, spatially accurate numerical method developed by the authors. We used a direct elliptic solver called the 'SEVP

(Stabilized Error Vector Propagation) Method' (Madala 1978) for the Poisson equation and an accurate integral-series formula (Sa & Chang 1990) for the far-boundary stream-function condition. In the present paper attention is directed to the vortex shedding patterns changing under the influence of buoyancy force, to the wall heat transfer from the cylinder, and finally to the breakdown of vortex shedding by the heating effect.

2. Governing equations and numerical methods

A viscous incompressible Boussinesq flow is assumed. A horizontal circular cylinder with radius a and of constant surface temperature T_w is placed transversely in an upward free stream of uniform velocity U as shown in figure 1. The conservation equations, first written in the cylindrical polar coordinates (r, θ), are transformed to the computational coordinates (ξ, η) by $r = e^{\pi\xi}$ and $\theta = \pi\eta$. The governing equations are then, in terms of vorticity, stream function, and temperature,

$$\frac{\partial\zeta}{\partial t}+\frac{1}{(\pi r)^2}\left(\frac{\partial}{\partial\xi}\left(\zeta\frac{\partial\psi}{\partial\eta}\right)-\frac{\partial}{\partial\eta}\left(\zeta\frac{\partial\psi}{\partial\xi}\right)\right)=\frac{2}{Re}\tilde{\nabla}^2\zeta-\frac{Gr}{2Re^2\pi r}\left[\frac{\partial\phi}{\partial\xi}\sin\theta+\frac{\partial\phi}{\partial\eta}\cos\theta\right], \tag{1}$$

$$\tilde{\nabla}^2\psi=-\zeta, \tag{2}$$

$$\frac{\partial\phi}{\partial t}+\frac{1}{(\pi r)^2}\left(\frac{\partial}{\partial\xi}\left(\phi\frac{\partial\psi}{\partial\eta}\right)-\frac{\partial}{\partial\eta}\left(\phi\frac{\partial\psi}{\partial\xi}\right)\right)=\frac{2}{Re\,Pr}\tilde{\nabla}^2\phi, \tag{3}$$

where

$$\tilde{\nabla}^2\equiv\frac{1}{(\pi r)^2}\left(\frac{\partial^2}{\partial\xi^2}+\frac{\partial^2}{\partial\eta^2}\right).$$

Four parameters are defined as

$$Re=\frac{(2a)\,U}{\nu},\quad Pr=\frac{\nu}{\alpha},$$

$$Gr=\frac{g\beta(T_w-T_\infty)(2a)^3}{\nu^2},\quad Nu=\frac{(2a)\,h}{\kappa}=-\frac{2}{\pi}\frac{\partial\phi}{\partial\xi}\bigg|_w.$$

The vorticity, ζ, the stream function, ψ, and the temperature, ϕ, are advanced in time by numerically integrating (1), (2) and (3). Central differencing is used for the spatial derivatives. In contrast, the contravariant velocity components in the convection terms of (1) and (3), ψ_ξ and ψ_η, are approximated by a fourth-order finite differencing called the Hermitian relation:

$$\psi_{\xi_{i-1,j}}+4\psi_{\xi_{i,j}}+\psi_{\xi_{i+1,j}}=\frac{3}{\Delta\xi}(\psi_{i+1,j}-\psi_{i-1,j})+O(\Delta\xi^4), \tag{4a}$$

$$\psi_{\eta_{i,j-1}}+4\psi_{\eta_{i,j}}+\psi_{\eta_{i,j+1}}=\frac{3}{\Delta\eta}(\psi_{i,j+1}-\psi_{i,j-1})+O(\Delta\eta^4). \tag{4b}$$

Equations (1) and (3) are solved by the Euler explicit finite difference scheme, and (2) by a direct elliptic solver, the SEVP method. The present unsteady problem requires a large number of time steps, and it is mandatory that an efficient non-

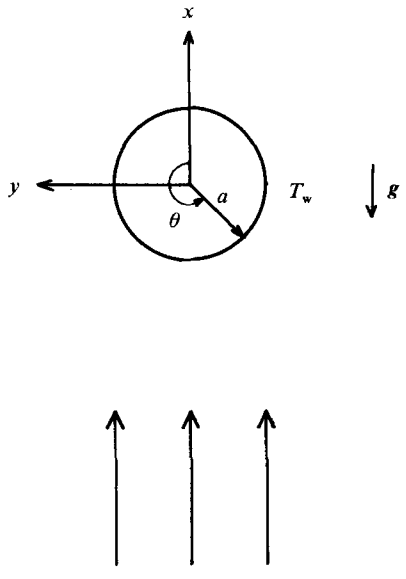

FIGURE 1. Flow geometry.

iterative elliptic solver is installed in the computer code. It should be noted that many earlier time-dependent computations on cylinder flow had to be confined to some initial starting motions or to the transient state before a fully periodic flow was brought in. The Error Vector Propagation (EVP) method (Roache 1975) is a direct method applicable to any type of elliptic equation. However, as shown by McAvaney & Leslie (1972), the EVP method is unstable when the number of grid points is large. Madala (1978) proposed a modification of this method, the SEVP (Stabilized EVP), which is stable for any number of grid points and retains most of the advantages of the earlier EVP. In the SEVP method, the integration region is divided into directional blocks, each of which is taken to be not large so that the EVP method remains stable. We have used a five-block SEVP method on the 51×50 grid system, with $\Delta\xi = 0.02$, $\Delta\eta = 0.04$ and $\Delta t = 0.05$.

Four boundaries of the computational domain shown in figure 1 require proper boundary conditions. An approximate form of the boundary data for the vorticity, the stream function, and the temperature would be, on $\xi = 0$,

$$\zeta_w = -\psi_\xi|_{w+1}/((\pi r)^2 \Delta\xi), \quad \psi_w = 0, \quad \phi_w = 1,$$

and on $\xi = \xi_{max}$,

$$\zeta = \phi = 0 \left(\text{at the inflow boundary where } \frac{\partial\psi}{\partial\eta} < 0\right),$$

$$\frac{\partial\zeta}{\partial\xi} = \frac{\partial\phi}{\partial\xi} = 0 \left(\text{at the outflow boundary where } \frac{\partial\psi}{\partial\eta} > 0\right),$$

$$\psi = \psi_{far} \text{ (over the entire boundary)},$$

On the cut boundaries, $\eta = 0$ and $\eta = \eta_{max}$, a periodic condition is enforced. In the above, ψ_{far} is the far-boundary stream function evaluated on the boundary of a finite computational domain by the integral-series method explained below.

We consider the Poisson equation (2) for the stream function. This can be transformed to a Poisson integral

$$\psi(\boldsymbol{r}) = Uy - Vx - \frac{1}{2\pi}\left[\iint_S \zeta_0 \ln(r')\,\mathrm{d}S_0 + \int_{C_w} V_{b_0} \ln(r')\,\mathrm{d}l_0\right]. \tag{5}$$

The last term in (5) is the wall velocity contribution in the counterclockwise direction; this line integral should then vanish if the wall stays stationary. As shown in Sa & Chang (1990), the stream function in (5) can be expanded at the far-field boundary as a power series of r^{-1}:

$$\psi_{\mathrm{far}} = Uy - Vx - \frac{F_0}{2\pi}\ln(r) + \frac{1}{2\pi}\sum_{n=1}^{3}\frac{1}{n}(F_n\cos(n\theta) + G_n\sin(n\theta))\,r^{-n} + O(r^{-4}), \tag{6}$$

where

$$F_0 = \iint \zeta\,\mathrm{d}S = 0,$$

$$F_1 = \iint \zeta x\,\mathrm{d}S, \qquad G_1 = \iint \zeta y\,\mathrm{d}S,$$

$$F_2 = \iint \zeta(x^2 - y^2)\,\mathrm{d}S, \qquad G_2 = \iint 2\zeta xy\,\mathrm{d}S,$$

$$F_3 = \iint \zeta(x^3 - 3xy^2)\,\mathrm{d}S, \quad G_3 = \iint \zeta(3x^2y - y^3)\,\mathrm{d}S.$$

In the present problem, an inequality $F_n \ll G_n$ holds because the alternating vortices shed from the circular cylinder have opposite signs. The right-hand side of (6) consists of the free-stream value of the stream function (the first two terms) plus the local correction terms made by the G_n and F_n contributions. The importance of these correction terms should not be underestimated when the computational domain has to be taken finite.

The lift and drag coefficients are defined by the equations

$$C_{\mathrm{L}} = \frac{\mathrm{Lift}}{\frac{1}{2}\rho U^2(2a)} = -\int p\sin\theta\,\mathrm{d}\theta + \frac{2}{Re}\int \zeta_{\mathrm{w}}\cos\theta\,\mathrm{d}\theta, \tag{7}$$

$$C_{\mathrm{D}} = \frac{\mathrm{Drag}}{\frac{1}{2}\rho U^2(2a)} = -\int p\cos\theta\,\mathrm{d}\theta - \frac{2}{Re}\int \zeta_{\mathrm{w}}\sin\theta\,\mathrm{d}\theta. \tag{8}$$

Integrations in the above are performed around the body surface. The wall pressure here is evaluated by the finite difference

$$p_{j+1} = p_j + \frac{\Delta\eta}{Re}\left(\left.\frac{\partial\zeta}{\partial\xi}\right|_j + \left.\frac{\partial\zeta}{\partial\xi}\right|_{j+1}\right),$$

which is an approximation of the following pressure condition to second order:

$$\frac{\partial p}{\partial\eta} = \frac{2}{Re}\frac{\partial\zeta}{\partial\xi}.$$

Experimental flow visualization requires various physical tracers such as hydrogen bubbles, tufts, smoke particles, and dyes. The numerical tracer adopted in the

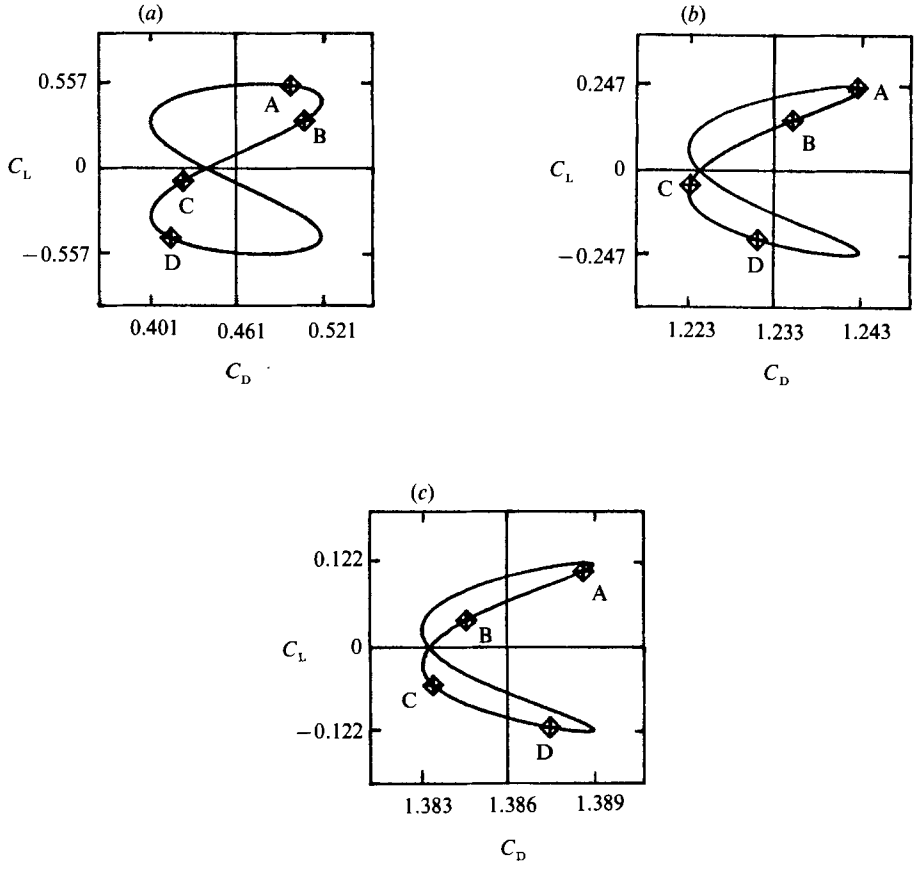

FIGURE 2. Phase relation between lift and drag coefficients at $Re = 100$: (*a*) $Gr = -5000$, (*b*) $Gr = 0$, (*c*) $Gr = 1000$. The phase angles in a cycle are A = 0, B = 1/8, C = 1/4, and D = 3/8 (t/T).

Classification	Contributors	C_D	*St*	*Nu*
Numerical	Present	1.233	0.155	5.23
	Jordan & Fromm (1972)	1.28	0.16	—
	Borthwick (1986)	1.215	—	—
	Jain & Goel (1976)	—	0.15	5.63
Experimental	Tritton (1959)	1.24	0.157/0.164	—
	Berger (1964)	—	0.155	—
	Eckert & Soehngen (1952)	—	—	5.23

TABLE 1. Comparison of drag coefficient, Strouhal number, and Nusselt number for an unheated cylinder

present study, point markers, was found to be a superior choice in visualizing the detailed structure of the near-wake vortices as was also demonstrated by Davis & Moore (1982) and Davis, Moore & Purtell (1984). The point markers were discharged at fourteen different locations in the rear part of the circular cylinder.

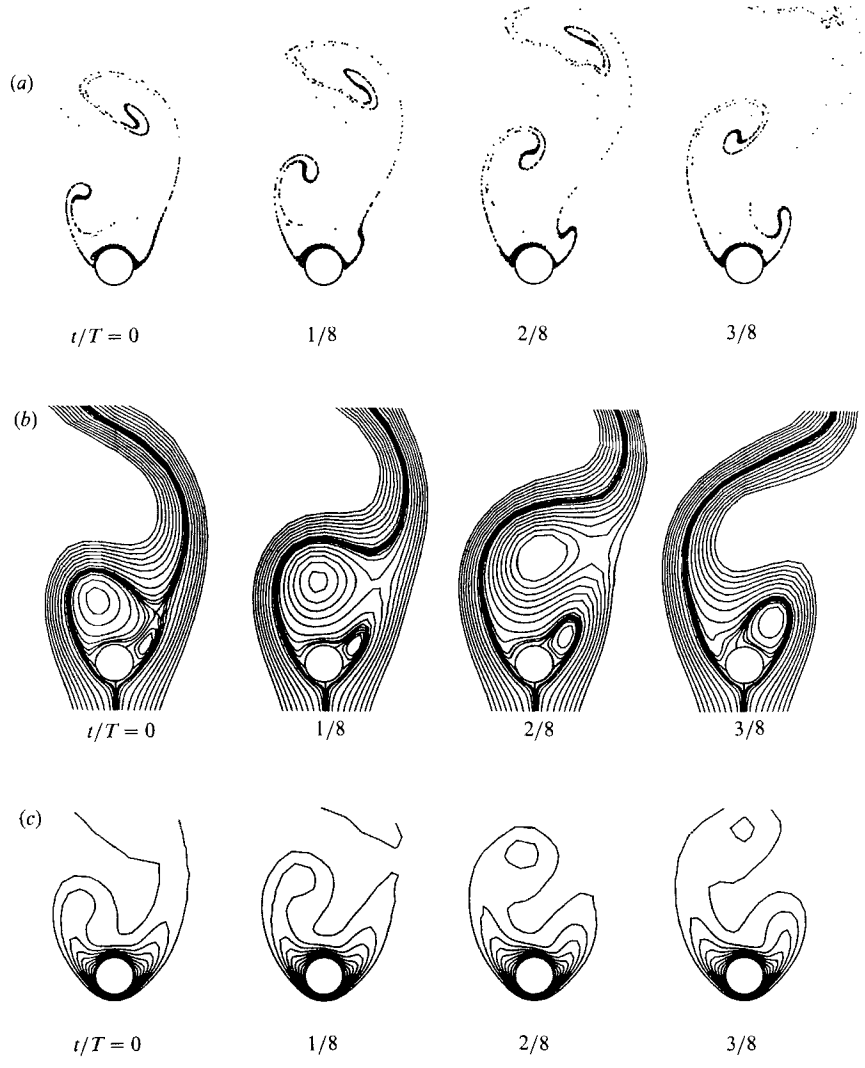

FIGURE 3. Periodic flow with vortex shedding at $Re = 100$, $Gr = -10000$: (*a*) streaklines, (*b*) streamlines, (*c*) isotherms.

3. Results and discussion

Before any discussion of the results, it is necessary to delineate the parameter range in which the Boussinesq approximation is justified, that is, $\beta\Delta T \leqslant 0.1$. It implies that, using the non-dimensional parameters,

$$Ri = \frac{Gr}{Re^2} = \frac{g\beta\Delta TD}{U^2} = \frac{\beta\Delta T}{F^2} \quad \left(:F^2 = \frac{U^2}{gD}\right),$$

the Froude number should be in the range $F^2 < 0.1/Ri$. The present results are then valid for small value of F or $\beta\Delta T$, which correspond to small U, large D, and small ΔT in the experiment.

The two mathematical features of the present paper, the Hermitian relation used for the contravariant velocity components in the convection terms of the vorticity transport equation and the integral-series formula of the far-field stream-function

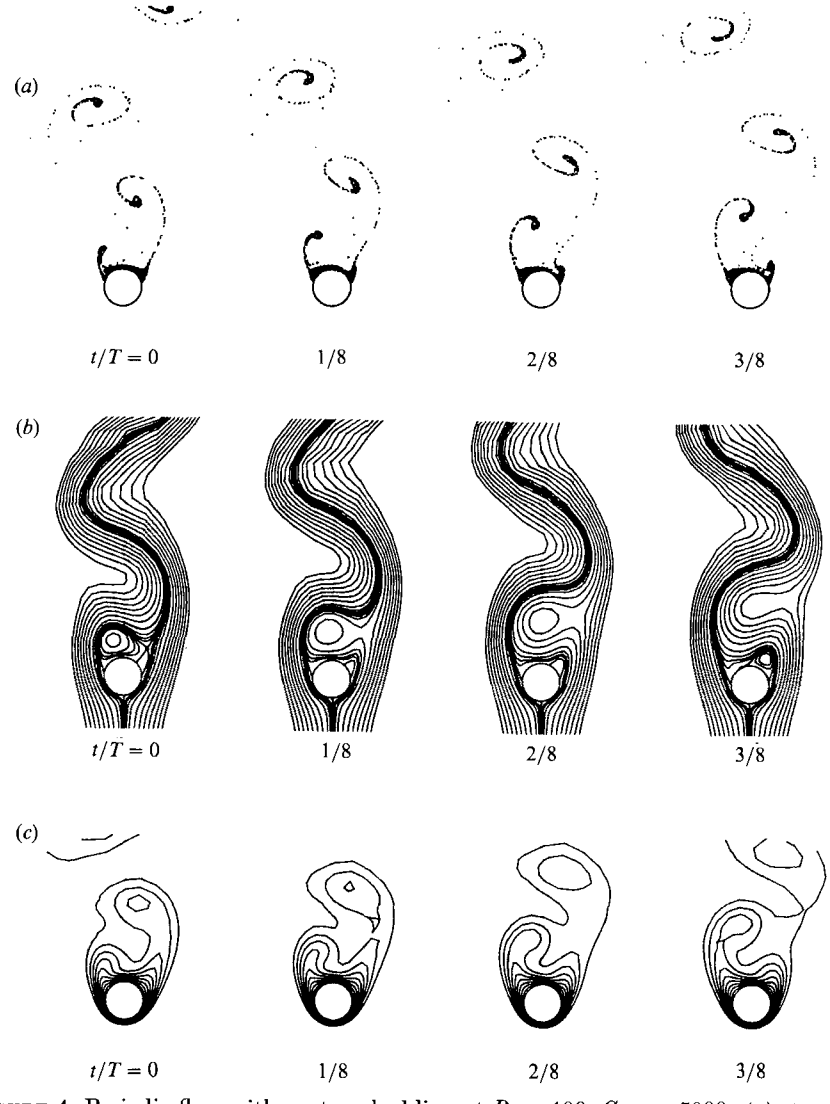

FIGURE 4. Periodic flow with vortex shedding at $Re = 100$, $Gr = -5000$: (*a*) streaklines, (*b*) streamlines, (*c*) isotherms.

condition, have allowed successful numerical simulation of the delicate vortex shedding phenomenon in the near wake of a circular cylinder. The direct elliptic solver applied to the Poisson equation of the stream function has also contributed to the efficient numerical solution of the otherwise lengthy computation. For an unheated cylinder ($Gr = 0$) at $Re = 100$, the averaged drag coefficient, the Strouhal number, and the averaged Nusselt number are found to be in good agreement with the earlier results, as shown in table 1. The present computation for a heated cylinder also showed the increase of shedding frequency and the subsequent breakdown of vortex shedding, which agreed well with other experimental and numerical results (Noto & Matsumoto 1985, 1987*a*; Jain & Lohar 1979).

Figure 2 presents the phase relation between the drag and the lift coefficients at $Gr = -5000$, 0, and 1000. The strict periodicity established in the present paper is well demonstrated by the curves of these aerodynamic coefficients. The strictly

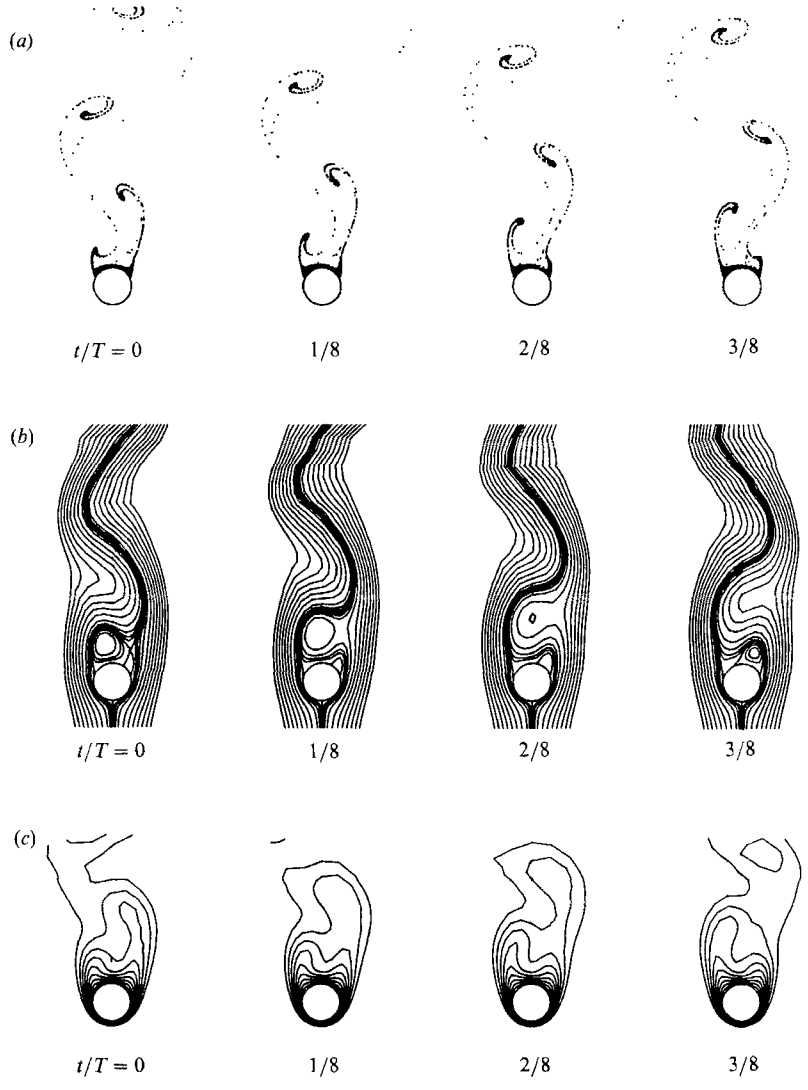

FIGURE 5. Periodic flow with vortex shedding at $Re = 100$, $Gr = -1000$: (*a*) streaklines, (*b*) streamlines, (*c*) isotherms.

periodic state is important in investigating the buoyancy effect on the vortex shedding. The Strouhal numbers to be presented later are actually evaluated using the temporal cycle of these phase curves.

The pattern of the ordinary vortex streets observable behind the (unheated) circular cylinder can be severely altered by the buoyancy force, with respect to the structure and size of the vortices, as presented in figures 3–7. The time sequence of the streaklines, streamlines, and isotherms plotted in these figures reveal the behaviour of the vortical flows under the thermal influence. As the cylinder is cooled below the environmental temperature ($Gr < 0$: figures 3–5), the strength of the shear layer increases and the roll-up process is more activated because the velocity in the wake region is reduced by the negative buoyancy force of the cold air. On the other hand, heating increases the velocity in the wake region and causes the shear layer to be weakened. As the Grashof number increases from zero in the positive direction,

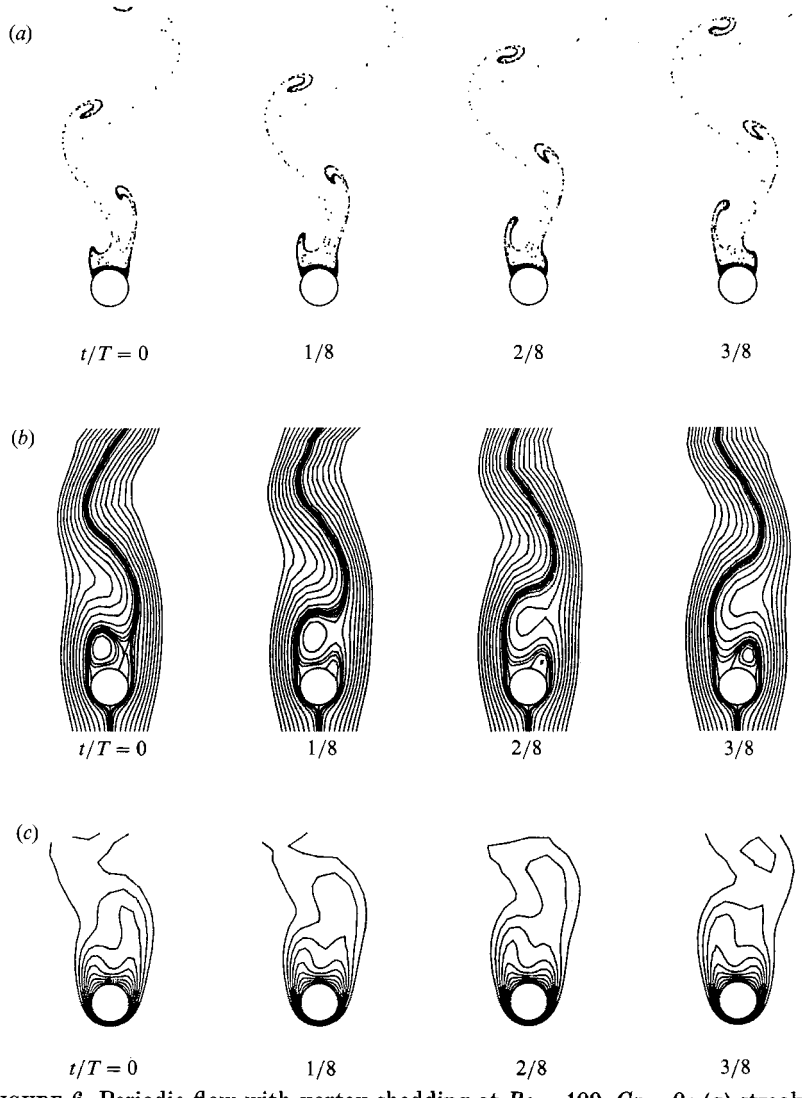

FIGURE 6. Periodic flow with vortex shedding at $Re = 100$, $Gr = 0$: (*a*) streaklines, (*b*) streamlines, (*c*) isotherms.

the entrainment of the ambient flow into the wake cavity diminishes and eventually vanishes at $Gr = 1500$. In the range of $Gr \geqslant 1500$, the stationary twin vortices are attached to the rear of the cylinder (see figures 8–11). The present study then distinguishes two different flow patterns: periodic flow for $Gr < 1500$ and steady flow with attached twin vortices for $Gr > 1500$. Here, the Grashof number of 1500 is the critical number between a periodic and a steady flow for $Re = 100$. For the strongly cooled cylinder, however, the separation point will leave the cylinder surface to move into the fluid: for example, see the case of $Re = 20$ with $Gr = -800$ in Badr (1984).

The Strouhal number ($St = f(2a)/U$) plotted in figure 12 indicates that the vortex shedding frequency f is heavily dependent on the Grashof number. Heating generally accelerates the wall boundary layer and increases the shedding frequency, while more stability is imparted to the vortex street in the wake region by the buoyancy force.

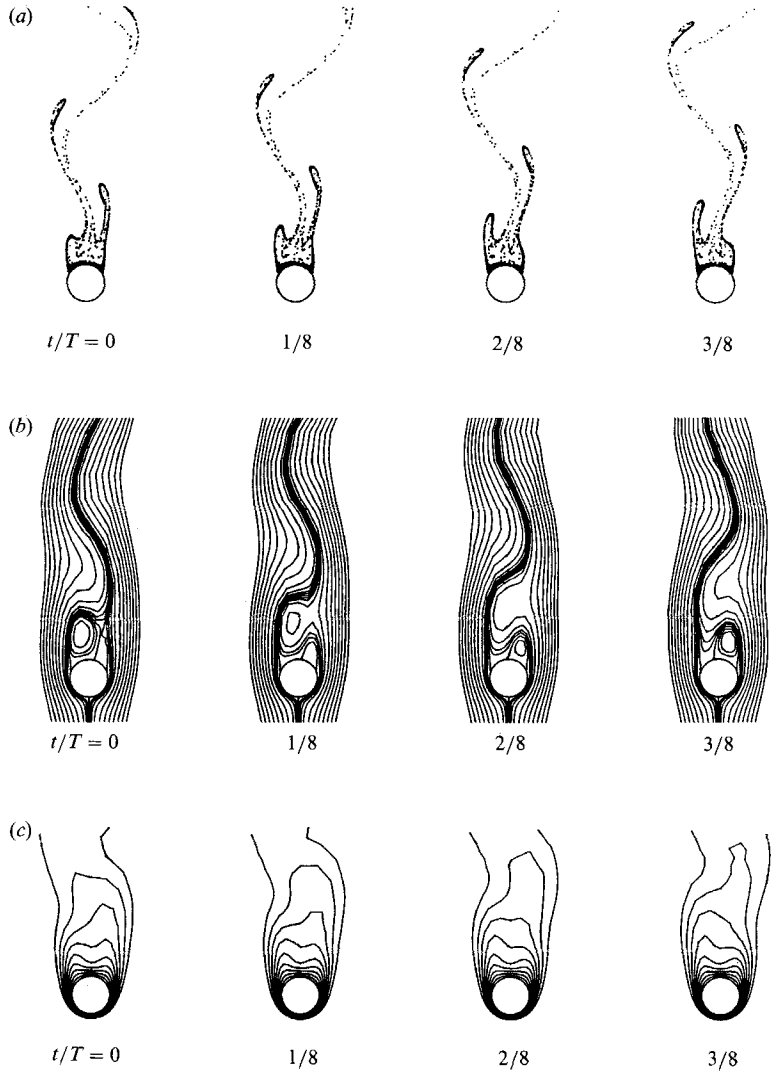

FIGURE 7. Periodic flow with vortex shedding at $Re = 100$, $Gr = 1000$: (*a*) streaklines, (*b*) streamlines, (*c*) isotherms.

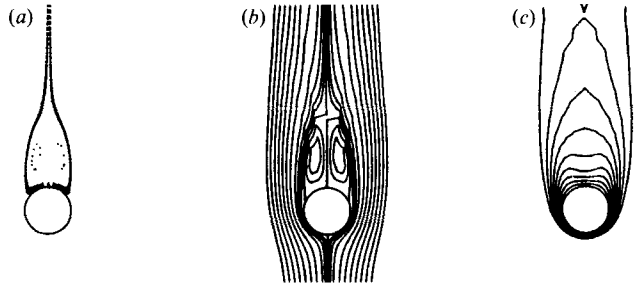

FIGURE 8. Steady flow with twin vortices at $Re = 100$, $Gr = 1500$: (*a*) streaklines, (*b*) streamlines, (*c*) isotherms.

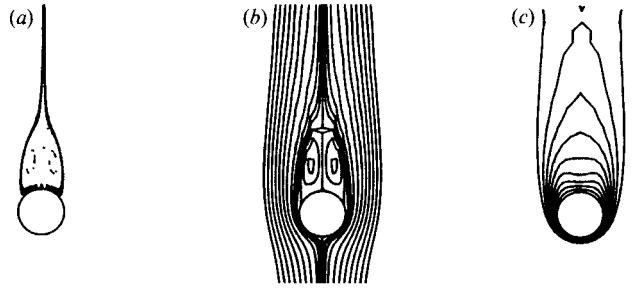

FIGURE 9. Steady flow with twin vortices at $Re = 100$, $Gr = 2000$: (*a*) streaklines, (*b*) streamlines, (*c*) isotherms.

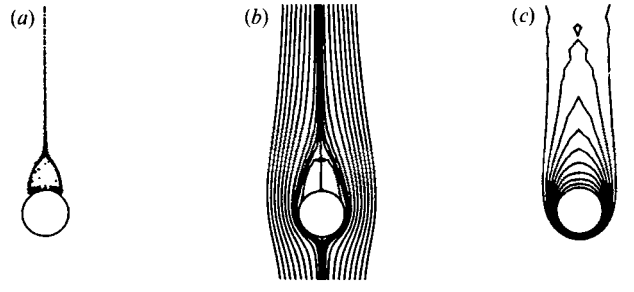

FIGURE 10. Steady flow with twin vortices at $Re = 100$, $Gr = 5000$: (*a*) streaklines, (*b*) streamlines, (*c*) isotherms.

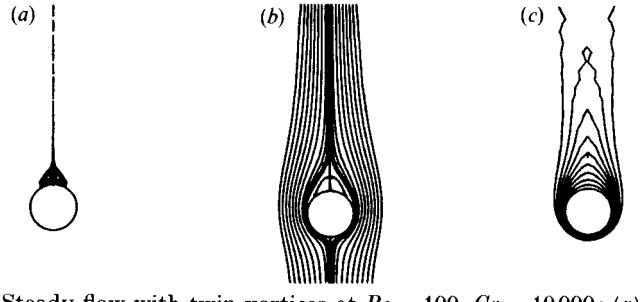

FIGURE 11. Steady flow with twin vortices at $Re = 100$, $Gr = 10000$: (*a*) streaklines, (*b*) streamlines, (*c*) isotherms.

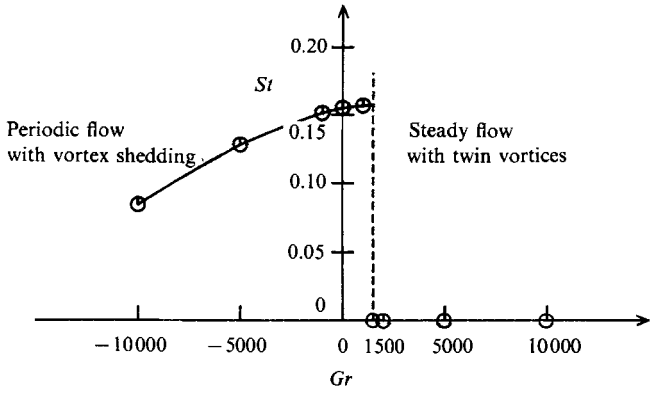

FIGURE 12. Strouhal number *vs.* Grashof number.

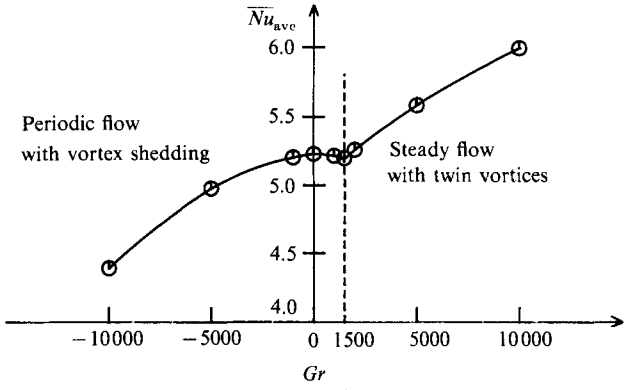

FIGURE 13. Temporal mean of the average Nusselt number *vs.* Grashof number.

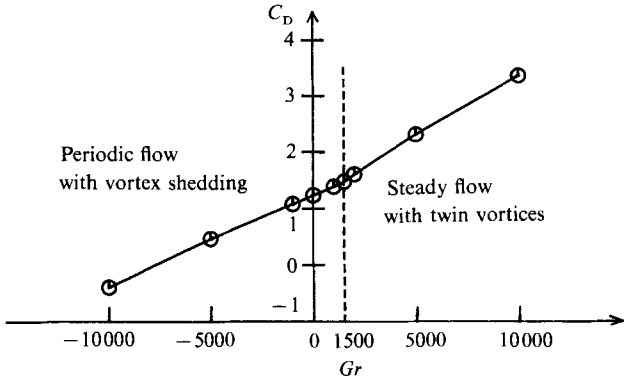

FIGURE 14. Drag coefficient *vs.* Grashof number.

A partial analogy for shedding frequency can be found between the heating and the increasing Reynolds number for an unheated cylinder; as Reynolds number increases, the wall boundary layer becomes thinner and accelerated although the vortex street is less stable in the wake region. For the case of a heated cylinder, the Strouhal number which is increasing monotonically with the Grashof number, astonishingly experiences a singular decay at the critical number $Gr = 1500$ as can be observed in figure 12. This sudden vanishing of dynamic vortices has been also experimentally observed by Noto & Matsumoto (1985) and they called it 'the breakdown of the Kármán vortex street'.

The temporal mean of the space-averaged Nusselt number, $\overline{Nu}_{ave}$, which is averaged over the cylinder surface and over a period of vortex shedding, is plotted in figure 13. In a steady-state convection problem, the wall heat transfer generally increases with the Grashof number. This trend, however, can be false in an unsteady flow regime where the flow structure is dynamically changed depending on the Grashof number, because the flow of entrainment during the vortex shedding is an important factor in the convective heat transfer from a bluff body. The slight reduction in the average Nusselt number to form a local minimum ahead of the discontinuity at $Gr = 1500$ in figure 13 is very characteristic of this changing flow pattern. Physically, for $500 < Gr < 1500$, the reduced entrainment of external fluid in the near-wake region owing to the weakened roll-up process of the vortex sheet is responsible for the local minimum of the average Nusselt number. However, for

$Gr \geqslant 1500$, with the stationary twin vortices attached to the cylinder, the convective heat transfer rate is again on the positive slope. The drag coefficient presented in figure 14 shows rather less sensitivity to the change of flow pattern. Only a slight discontinuity in the slope of the drag curve is observed at $Gr = 1500$.

4. Concluding remarks

The present numerical study, aimed at time efficiency as well as spatial accuracy in computing the near-wake vortices behind a circular cylinder, has allowed a detailed investigation of the buoyancy effects in mixed convection. The role of heating has been found not only to accelerate the wall boundary layer but also to increase the velocity in the wake region. As the Grashof number increases, therefore, the thinner boundary layer causes the shedding frequency to increase, while the weakened roll-up process reduces the entrainment of the ambient flow into the wake cavity until the dynamic vortices finally degenerate.

It is interesting to observe the behaviour of the shedding frequency, the drag coefficient, and the convective heat transfer, due to the buoyant effect. The shedding frequency and the shedding pattern depend on the thickness of the wall boundary layer and the strength of the vortex sheet in the near-wake region, respectively. The drag coefficient hardly seems to be influenced by the reduced entrainment, but has a change of slope when the periodic flow changes into a steady flow. The Nusselt number, however, is found very sensitive to the reduced entrainment because it is dependent on the flow convection near the cylinder. At $Gr < 500$, since the separated region on the wall becomes narrow and the wall boundary layer is accelerated as the Grashof number increases, the Nusselt number increases monotonically. At $500 < Gr < 1500$, the substantially reduced entrainment of fresh cold air due to the weakened roll-up process causes the convective heat transfer rate to decrease. In the steady flow with twin vortices, the Nusselt number again increases monotonically with the Grashof number because of the decrease of the separation bubble size and the acceleration of the wall boundary layer.

REFERENCES

BADR, H. M. 1984 Laminar combined convection from a horizontal cylinder – parallel and contra flow regimes. *Intl J. Heat Mass Transfer* **27**, 15.

BERGER, E. 1964 Bestimmung der hydrodynamischen Groessen einer Karmanschen Wirbelstrasse aus Hitzdrahtmessungen bei kleinen Reynoldsschen Zahlen. *Z. Flugwiss.* **12**, 41.

BERGER, E. & WILLE, R. 1972 Periodic flow phenomena. *Ann. Rev. Fluid Mech.* **4**, 313.

BORTHWICK, A. 1986 Comparison between two finite-difference schemes for computing the flow around a cylinder. *Intl J. Num. Meth. Fluids* **6**, 275.

DAVIS, R. W. & MOORE, E. F. 1982 A numerical study of vortex shedding from rectangles. *J. Fluid Mech.* **110**, 475.

DAVIS, R. W., MOORE, E. F. & PURTELL, L. P. 1984 A numerical-experimental study of confined flow around rectangular cylinders. *Phys. Fluids* **27**, 46.

ECKERT, E. R. G. & SOEHNGEN, E. 1952 Distribution of heat transfer coefficients around circular cylinder in cross flow at Reynolds numbers 20 to 500. *Trans. ASME* **74**, 343.

JAIN, P. C. & GOEL, B. S. 1976 A numerical study of unsteady laminar forced convection from a circular cylinder. *Trans. ASME* C: *J. Heat Transfer* **98**, 303.

JAIN, P. C. & LOHAR, B. L. 1979 Unsteady mixed convection heat transfer from a horizontal circular cylinder. *Trans. ASME* C: *J. Heat Transfer* **101**, 126.

JORDAN, S. K. & FROMM, J. E. 1972 Oscillating drag, lift, and torque on a circular cylinder in a uniform flow. *Phys. Fluids* **15**, 371.

MADALA, R. V. 1978 An efficient direct solver for separable and non-separable elliptic equations. *Mon. Weath. Rev.* **106**, 1735.

MCAVANEY, B. J. & LESLIE, L. M. 1972 Comments on a direct solution of Poisson's equation by generalized sweep-out method. *J. Met. Soc. Japan* **50**, 136.

NOTO, K. & MATSUMOTO, R. 1985 A breakdown of the Kármán vortex street due to the natural convection. In *Flow Visualization III*, p. 348. Springer.

NOTO, K. & MATSUMOTO, R. 1987*a* Numerical simulation on development of the Kármán vortex street due to the negative buoyant force. In *Numerical Methods in Laminar and Turbulent Flow 5*, p. 796. Pineridge.

NOTO, K. & MATSUMOTO, R. 1987*b* Breakdown of the Kármán vortex street due to natural convection (case from an elliptic cylinder whose major axis oriented at right angle to main stream). In *Numerical Methods in Thermal Problems 5*, p. 484. Pineridge.

OOSTHUIZEN, P. H. & MADAN, S. 1971 The effect of flow direction on combined convective heat transfer from cylinders to air. *Trans. ASME* C: *J. Heat Transfer* **93**, 240.

ROACHE, P. J. 1975 *Computational Fluid Dynamics*. Hermosa.

SA, J. Y. & CHANG, K. S. 1990 On far-field stream function condition for two-dimensional incompressible flows. *J. Comput. Phys.*, to appear.

TRITTON, D. J. 1959 Experiments on the flow past a circular cylinder at low Reynolds numbers. *J. Fluid Mech.* **6**, 547.